

Tunable One-Pot Syntheses of Hexagonal-, Cubic-, and Lamellar-Mesostructured Vanadium–Phosphorus Oxides

Noritaka Mizuno,* Hiroshi Hatayama, Sayaka Uchida, and Akira Taguchi

Department of Applied Chemistry, School of Engineering, The University of Tokyo,
Hongo, Bunkyo-ku, Tokyo 113-8656, Japan

Received June 30, 2000. Revised Manuscript Received October 23, 2000

Hexagonal-, cubic-, and lamellar-mesostructured vanadium–phosphorus oxides were hydrothermally synthesized by using V metal as a reducing agent and a V source. The respective phases were tunably synthesized in the ranges of pH 2.63–2.95, 3.00–3.36, and 3.45–4.45. It is suggested that the formation of these mesostructured materials depends on the solution species of vanadium and phosphorus. The unit cell constants of hexagonal, cubic, and lamellar phases were determined to be $a = 5.05$ nm, $a = 8.54$ nm, and $c = 3.22$ nm, respectively. IR spectroscopy, XRD, and elemental analyses show that hexagonal- and cubic-mesostructured materials possess an amorphous wall of vanadium–phosphorus oxides and their P/V ratios were 0.99 and 0.76, respectively. On the other hand, the lamellar mesostructured material possessed more crystalline layers of vanadium–phosphorus oxide with a P/V ratio of 0.50. The cetyltrimethylammonium templates could be exchanged with K^+ or Cs^+ .

Introduction

Much effort has been devoted to synthesizing mesoporous vanadium–phosphorus–oxides (abbreviated by V–P–Os). To date, hexagonally mesostructured V–P–Os have successfully been synthesized and characterized.^{1–3} However, nothing is known of the tunable synthesis of hexagonal-, cubic-, and lamellar-phased V–P–Os.

Surfactant templating methods for syntheses of hexagonal (MCM-41), cubic (MCM-48), and lamellar (MCM-50) mesoporous silicas have first been reported by the researchers of Mobil Oil Co.^{4,5} Not only the application to the catalysis and host–guest chemistry but also the improvement and optimization of synthetic conditions have been investigated.^{6–8} The majority of publication in this area has concentrated on the hexagonal MCM-41 while the phase transition of MCM materials with the synthetic conditions⁹ and compositions^{4,5,10,11} has been reported.

These unique methods for developing siliceous mesoporous materials were applied to non-silica-based me-

sostructured materials such as single-metal oxides of Al,^{12,13} Ti,¹⁴ V,¹⁵ W,^{6,16} and Nb¹⁷ and binary oxides of Al–B,¹⁸ Al–P,¹⁹ and Zr–P.²⁰ Hexagonal and lamellar phases have been reported for various oxides so far, while cubic phases have been reported only for oxides of Nb,¹⁷ Sb,⁶ Al–B,¹⁸ and Zr.²¹ Therefore, little is known of the tunable syntheses of hexagonal-, cubic-, and lamellar-mesostructured phases except for siliceous MCM and SBA series.^{4–6}

(VO)₂P₂O₇ is an active phase or component for the industrialized oxidation of *n*-butane into maleic anhydride.^{22–25} We have previously communicated the one-pot hydrothermal synthesis of VOHPO₄·0.5H₂O, a catalyst precursor of (VO)₂P₂O₇, by using V metal not only as a V source but also as a reducing agent for V₂O₅. The

* To whom all correspondence should be addressed. Fax: +81-3-5841-7220. Phone: +81-3-5841-7275.

- (1) Abe, T.; Taguchi, A.; Iwamoto, M. *Chem. Mater.* **1995**, *7*, 1429.
- (2) Doi, T.; Miyake, T. *Chem. Commun.* **1996**, 1635.
- (3) Haskouri, J. E.; Roca, M.; Cabrera, S.; Alamo, J.; Beltrán-Porter, A.; Beltrán-Porter, D.; Marcos, M. D.; Amorós, P. *Chem. Mater.* **1999**, *11*, 1446.
- (4) Kresge, C. T.; Leonowicz, M. E.; Roth, W. J.; Vartuli, J. C.; Beck, J. S. *Nature* **1992**, *359*, 710.
- (5) Beck, J. S.; Vartuli, J. C.; Roth, W. J.; Leonowicz, M. E.; Kresge, C. T.; Schmitt, K. D.; Chu, C. T.-W.; Olson, D. H.; Sheppard, E. W.; McCullen, S. B.; Higgins, J. B.; Schlenker, J. L. *J. Am. Chem. Soc.* **1992**, *114*, 10834.
- (6) Huo, Q.; Margolese, D. I.; Ciesla, U.; Demuth, D. G.; Feng, P.; Gier, T. E.; Sieger, P.; Firouzi, A.; Chmelka, B. F.; Schüth, F.; Stucky, G. D. *Chem. Mater.* **1994**, *6*, 1176.
- (7) Sayari, A. *Chem. Mater.* **1996**, *8*, 1840.
- (8) Corma, A. *Chem. Rev.* **1997**, *97*, 2373.
- (9) Gallis, K. W.; Landry, C. C. *Chem. Mater.* **1997**, *9*, 2035.

- (10) Vartuli, J. C.; Schmitt, K. D.; Kresge, C. T.; Roth, W. J.; Leonowicz, M. E.; McCullen, S. B.; Hellring, S. D.; Beck, J. S.; Schlenker, J. L.; Olson, D. H.; Sheppard, E. W. *Chem. Mater.* **1994**, *6*, 2317.
- (11) Romero, A. A.; Alba, M. D.; Zhou, W.; Klinowski, J. *J. Phys. Chem. B* **1997**, *101*, 5294.
- (12) Vaudry, F.; Khodabandeh, S.; Davis, M. E. *Chem. Mater.* **1996**, *8*, 1451.
- (13) Holland, B. T.; Isbester, P. K.; Blanford, C. F.; Munson, E. J.; Stein, A. *J. Am. Chem. Soc.* **1997**, *119*, 6796.
- (14) Antonelli, D. M. *Microporous Mesoporous Mater.* **1999**, *30*, 315.
- (15) Luca, V.; Hook, J. M. *Chem. Mater.* **1997**, *9*, 2731.
- (16) Stein, A.; Fendorf, M.; Jarvie, T. P.; Mueller, K. T.; Benesi, A. J.; Mallouk T. E. *Chem. Mater.* **1995**, *7*, 304.
- (17) Antonelli, D. M.; Nakahira, A.; Ying, J. Y. *Inorg. Chem.* **1996**, *35*, 3126.
- (18) Ayyappan, S.; Rao, C. N. R. *Chem. Commun.* **1997**, 575.
- (19) Kimura, T.; Sugahara, Y.; Kuroda, K. *Chem. Commun.* **1998**, 559.
- (20) Ciesla, U.; Schacht, S.; Stucky, G. D.; Unger, K. K.; Schüth, F. *Angew. Chem., Int. Ed. Engl.* **1996**, *35*, 541.
- (21) Neeraj, S.; Rao, C. N. R. *J. Mater. Chem.* **1998**, *8*, 1631.
- (22) Hondnett, B. K. *Catal. Rev.-Sci. Eng.* **1985**, *27*, 373.
- (23) Centi, G.; Trifiro, F.; Ebner, J. R.; Franchetti, V. M. *Chem. Rev.* **1988**, *88*, 55.
- (24) Bordes, E. *Catal. Today* **1987**, *1*, 499.
- (25) Hutchings, G. J. *Appl. Catal.* **1991**, *72*, 1.

addition of cetyltrimethylammonium chloride promoted a high growth of (001) phase of $\text{VOHPO}_4 \cdot 0.5\text{H}_2\text{O}$.²⁶

Here, we apply the synthetic method of $\text{VOHPO}_4 \cdot 0.5\text{H}_2\text{O}$ to the syntheses of mesostructured V–P–Os by changing the pH with cetyltrimethylammonium hydroxide/chloride ratios and find the tunable one-pot hydrothermal syntheses of hexagonal-, cubic-, and lamellar-mesostructured V–P–Os by changing the pH with cetyltrimethylammonium hydroxide/chloride ratios.

Experimental Section

Syntheses. The reagents were commercially obtained and used without further purification. V–P–Os of hexagonal-, cubic-, and lamellar-phased mesostructured materials were synthesized as follows. To aqueous solution of cetyltrimethylammonium hydroxide/chloride ($\text{C}_{16}\text{TMA}(\text{OH}, \text{Cl})$, 30 mL, $0.67 \text{ mol} \cdot \text{dm}^{-3}$, Tokyo Kasei Co.), 2.31 g of 85% H_3PO_4 (Nacalai Tesque) was added and the resulting solution was stirred at room temperature. Then, V_2O_5 (1.46 g, Nacalai Tesque) and V metal (0.204 g, Mitsuwa Chemical) were dissolved and the solution was stirred for 1 h. Typical synthetic conditions were as follows. A molar composition of reaction solution was 1.0:2.0:5.0:5.0:420/ V: V_2O_5 : H_3PO_4 : $\text{C}_{16}\text{TMA}(\text{OH}, \text{Cl})$: H_2O . The pH of the solution was adjusted to an appropriate value (2.63–4.45) with diluted HCl. Thirty milliliters of the supernatant was placed into a 40 mL Teflon vessel mounted in an autoclave and hydrothermally treated at 473 K for 48 h. After cooling to room temperature, the precipitate was filtered and washed with $\approx 700 \text{ mL}$ of deionized water followed by evacuation at room temperature for 5 h. The colors of hexagonal-, cubic-, and lamellar-mesostructured V–P–Os were dark green, moss green, and bluish green, respectively. The respective typical yields were ≈ 6 , 4, and 4% on V-bases. Hereafter, hexagonal-, cubic-, and lamellar-mesostructured V–P–Os were abbreviated by HVPO, CVPO, and LVPO, respectively.

Ion Exchange. The ion exchanges of C_{16}TMA with alkali metal cations such as K^+ and Cs^+ were performed in air as follows. To the mixed solution of H_2O and ethanol (50 mL, v/v = 1:1), alkali metal chloride (50 mmol) was dissolved. Then, 0.05–0.1 g of LVPO was added and the suspension was stirred at room temperature for 2 h. After filtration, the resulting solid was washed with deionized water followed by evacuation at room temperature for 5 h.

Characterization. The powder X-ray diffraction (XRD) patterns were recorded on a powder X-ray diffractometer (MAC Science Co., MXP³) by using $\text{CuK}\alpha$ radiation. The infrared spectra of KBr pellets were recorded on a Perkin-Elmer Paragon 1000PC spectrometer. Transmission electron micrographs (TEM) were measured with JEOL JEM-4000 FXII. The chemical formulas of the products were determined by ICP (Shimadzu, ICPS-8000) and CHN (Yanaco, CHN CORDER MT-5) analyses. Thermogravimetric analysis (TGA) was carried out at a heating rate of 1 K min^{-1} in a N_2 flow ($250 \text{ cm}^3 \text{ min}^{-1}$) with Seiko instruments TG/DTA 220. MAS NMR spectra were measured with a Chemagnetics CMX-300 Infinity spectrometer operating at 7.05 T. The sample was set into a zirconia rotor (7.5 mm in diameter). ^1H (300 MHz) and ^{13}C (75.6 MHz) MAS NMR spectra were recorded using single-pulse excitation. The MAS rate was 5 kHz and the measurements were carried out at 298 K. Hexamethylbenzene (^{13}C : 17.17 ppm) and adamantane (^1H : 1.91 ppm) were used as external standards.

Temperature-programmed desorption was carried out at a heating rate of 1 K min^{-1} by using a commercial TPD system (BEL Japan Inc., Multitask TPD) equipped with a quadrupole mass spectrometer (TPD mass). After the sample ($\approx 80 \text{ mg}$) was pretreated in a He flow at 303 K for 1 h, the sample was heated to 650 K at a rate of 1 K min^{-1} . The m/e numbers of

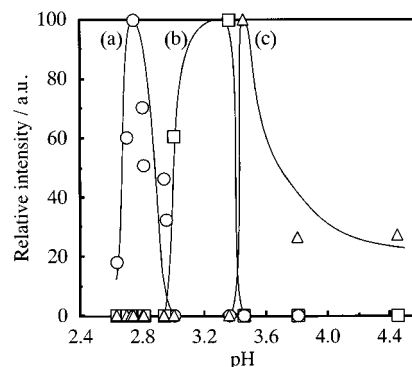


Figure 1. Dependence of XRD peak intensities of mesostructured V–P–Os on the pH of the synthetic solution: (a) HVPO; (b) CVPO; (c) LVPO. The most intense signal intensities are taken as unity.

18, 29, and 44 were detected and used as a measure of desorption of H_2O and C_{16}TMA from samples.

The average oxidation state of vanadium in the samples was determined by double titration according to the literature.²⁷ About 50 mg of mesostructured V–P–Os was dissolved in 50 mL of 1 M H_2SO_4 . The $\text{V}^{3+} + \text{V}^{4+}$ content in the sample was determined by titration (volume 1) with an aqueous solution of KMnO_4 (0.01 M). An aqueous solution (25 mL) of $\text{FeSO}_4 \cdot (\text{NH}_4)_2\text{SO}_4 \cdot 6\text{H}_2\text{O}$ (4.5 g, 0.011 mol) was then added to reduce all the V^{3+} to V^{4+} . The solution was cooled in an ice bath. An excess of $(\text{NH}_4)_2\text{S}_2\text{O}_8$ (3.9 g, 0.017 mol) was added to oxidize Fe^{2+} to Fe^{3+} . Finally, V^{4+} was titrated (volume 2) with KMnO_4 (0.01 M) to measure the total vanadium content of the sample. The average volume of vanadium was calculated by $5 - (\text{volume 1})/(\text{volume 2})$.

Results and Discussion

Tunable Syntheses of Hexagonal-, Cubic-, and Lamellar-Mesostructured Materials. The formation of HVPO, CVPO, and LVPO depended on the pH of the synthetic solution. The changes of the most intense signal intensities are shown in Figure 1. The respective phases were tunably synthesized in the ranges of pH 2.63–2.95, 3.00–3.36, and 3.45–4.45.²⁸ The single phase of HVPO was obtained at pH 2.74. The products were changed to CVPO and LVPO by increasing the pH and the single phases of CVPO and LVPO were prepared at pH 3.36 and 3.45, respectively.

The XRD patterns are shown in Figure 2. Each line in Figure 2 (a–c) can be assigned to HVPO, CVPO, and LVPO, respectively, while the details will be described in the next section. These results demonstrate the first tunable synthesis of hexagonal-, cubic-, and lamellar-mesostructured V–P–Os by changing the pH of the synthetic solution. The order of hexagonal \rightarrow cubic \rightarrow lamellar phase formation with increasing pH was also reported for silica MCMs by Romero et al.¹¹ Similarly, hexagonal \rightarrow cubic and hexagonal \rightarrow cubic \rightarrow lamellar phase transitions with an increase in pH were reported for Sb^6 and Al-B^{18} oxides, respectively. The structures of micelles for cationic surfactants changed in the order of hexagonal \rightarrow cubic \rightarrow lamellar phases with an increase in pH.²⁹ The phase transformation with pH was the same as those of the present system. Therefore, the

(27) Hodnett, B. K.; Permanne, P.; Delmon, B. *Appl. Catal.* **1983**, *6*, 231.

(28) Vanadium phosphate hemihydrate ($\text{VOHPO}_4 \cdot 0.5\text{H}_2\text{O}$) was formed in the pH range 0.85–2.13. The details will be reported in due course.

(26) Mizuno, N.; Hatayama, H.; Misono, M. *Chem. Mater.* **1997**, *9*, 2697.

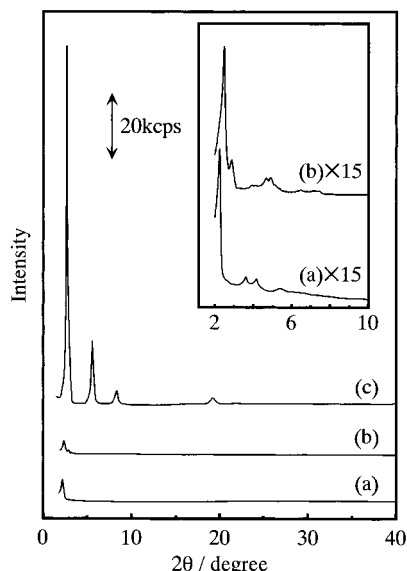


Figure 2. XRD patterns of mesostructured V-P-Os: (a) HVPO; (b) CVPO; (c) LVPO. Inset: Expanded XRD patterns of HVPO and CVPO.

change in micelle structure was the reason for the phase transformation of the V-P-O system.

It is known that tetravalent vanadium exists as $\text{VO}(\text{H}_2\text{O})_5^{2+}$ in an acidic aqueous solution.³⁰ According to the partial charge model, the predominant species below pH 2.6 is $\text{VO}(\text{H}_2\text{O})_5^{2+}$.^{31,32} The hydrolysis and condensation with an increase in pH leads to the formation of $\text{VO}(\text{OH})(\text{H}_2\text{O})_4^+$ and $(\text{VO})_2(\text{OH})_2(\text{H}_2\text{O})_6^{2+}$. Phosphoric acid exists as PO_4^{3-} , HPO_4^{2-} , H_2PO_4^- , and H_3PO_4 . The respective ratios are 3.3×10^{-15} : 3.1×10^{-5} : 1.0 : 2.6×10^{-1} at pH 2.7 and 8.3×10^{-14} : 1.6×10^{-4} : 1.0 : 5.3×10^{-2} at pH 3.4,³³ and H_2PO_4^- is the major species. Therefore, the formation of vanadium-phosphorus and C_{16}TMA -phosphorus complexes such as $[\text{VO}(\text{H}_2\text{O})_4][(\text{H}_2\text{PO}_4)]^+$, $[\text{VO}(\text{OH})(\text{H}_2\text{O})_4][\text{H}_2\text{PO}_4]$, $[(\text{VO})_2(\text{OH})_2(\text{H}_2\text{O})_6][(\text{H}_2\text{PO}_4)]^+$, and $[\text{C}_{16}\text{TMA}][\text{H}_2\text{PO}_4]$ is probable. These complexes may be precursors of walls of V-P-Os.

I. Hexagonal-Mesostructured V-P-O. When the pH was adjusted to 2.8 with aqueous ammonia or trimethylamine instead of $\text{C}_{16}\text{TMAOH}$, no hexagonal phase was formed. This shows that $\text{C}_{16}\text{TMAOH}$ was a good pH adjusting reagent for the formation of HVPO.

The hexagonal phase was not formed at 373 K, but started to be formed from 413 K. The XRD signal intensity of (001) reflection increased with an increase in the synthetic temperature from 373 to 473 K and reached a maximum at 473 K. Hereafter, HVPO synthesized with $\text{C}_{16}\text{TMA}(\text{OH}, \text{Cl})$ at pH 2.74 and 473 K is characterized.

The IR spectrum of HVPO is shown in Figure 3a. The IR bands were observed at 3422 and 1654 cm^{-1} , assignable to $\nu(\text{OH})$ and $\delta(\text{H}_2\text{O})$, respectively. This fact shows

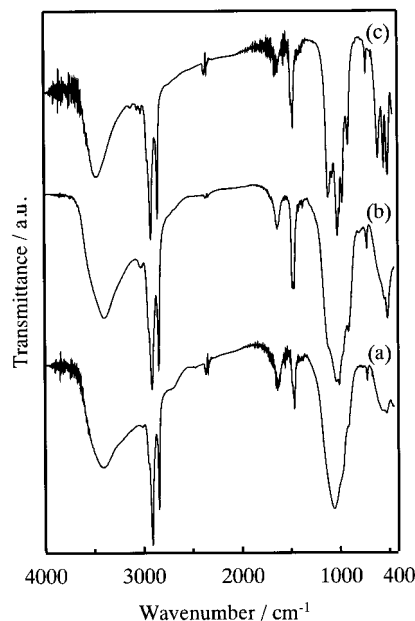


Figure 3. IR spectra of mesostructured V-P-Os: (a) HVPO; (b) CVPO; (c) LVPO.

the presence of water molecules. Regarding the organic molecules, five IR bands were observed at 3018, 2954 (shoulder), 2919, 2851, and 1467 cm^{-1} . The positions were in fair agreement with those of $\text{C}_{16}\text{TMACl}$, showing the presence of C_{16}TMA cations. The presence of water and C_{16}TMA molecules was also observed for CVPO and LVPO. In the range of 1300–500 cm^{-1} , the spectrum of HVPO exhibited a broad absorption band around 1000 cm^{-1} , suggesting that the wall of HVPO is amorphous V-P-O.^{1,4,5}

The amounts of V, P, C, H, N, and O in HVPO were 13.0, 7.8, 35.5, 7.1, 2.1, and 34.5 wt %, respectively, as listed in Table 1. The atomic P/V ratio was almost 1.00 and the average valence of V was 4.25. On the basis of these data, the chemical formula of HVPO was estimated to be $\{\text{C}_{16}\text{H}_{33}\text{N}(\text{CH}_3)_3\}_{0.60}\text{VP}_{0.99}\text{O}_{4.90} \cdot 3.45\text{H}_2\text{O}$.

TGA and TPD mass spectra of HVPO are shown in Figure 4a. Below 523 K desorption of water ($m/e = 18$) was only observed and the corresponding weight loss in the range of 298–523 K was 15 wt %, while the weak signals such as $m/e = 29$ and 44 corresponding to the decomposition of C_{16}TMA were observed above 523 K. The water content of 15 wt % was in agreement with 15.8 wt % in the chemical formula.

Figure 2a shows the XRD pattern of HVPO prepared at pH 2.74. Four low-angle signals were observed at $2\theta = 2.02^\circ$, 3.58° , 4.11° , and 5.47° , corresponding to hexagonal (100), (110), (200), and (210) reflections, respectively. The unit cell constant (a) was 5.05 nm ($2 \times d_{100}/\sqrt{3}$), which was slightly larger than those reported by Abe et al. (4.57 nm)¹ and Haskouri et al. (4.28–4.67 nm)³ using the same surfactant (C_{16}TMA). It is noted that the XRD pattern of HVPO contained a halo pattern around $2\theta = 20^\circ$.^{1,4,5} The appearance of the halo XRD pattern is consistent with the broad IR band around 1000 cm^{-1} .

The regular hexagonal array of inorganic wall and surfactant micelles was confirmed by the TEM measurement as shown in Figure 5a. The distance between pore centers was 4.3 ± 0.2 nm, a little smaller than 5.05

(29) Israelachvili, J. N. *Intermolecular and Surface Forces*; Academic Press Ltd.: London, 1992.

(30) Baes, C. F.; Mesmer, R. E. *The Hydrolysis of Cations*; John Wiley and Sons: New York, 1976.

(31) Livage, J.; Henry, M.; Sanchez, C. *Prog. Solid State Chem.* **1988**, *18*, 259.

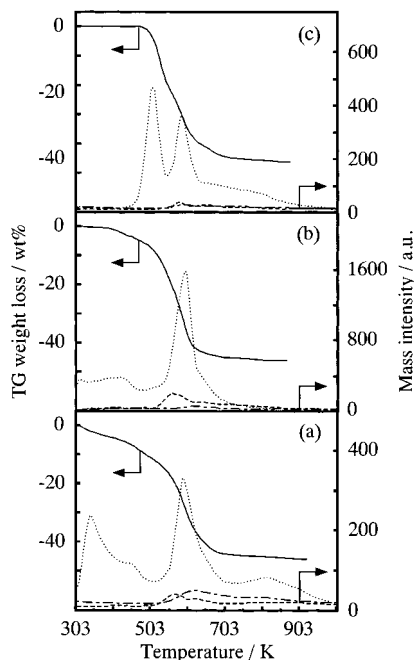
(32) Roca, M.; Marcos, M. D.; Amorós, P.; Beltrán-Porter, A.; Edwards, A. J.; Beltrán-Porter, D. *Inorg. Chem.* **1996**, *35*, 5613.

(33) The ratios were calculated with $[\text{H}_3\text{PO}_4] + [\text{H}_2\text{PO}_4^-] + [\text{HPO}_4^{2-}] + [\text{PO}_4^{3-}] = 0.668$ M, $\text{p}K_{a1} = 2.12$, $\text{p}K_{a2} = 7.21$, and $\text{p}K_{a3} = 12.67$ at 298 K.

Table 1. Elemental Analysis, Valence of Vanadium, and Composition for HVPO, CVPO, and LVPO

product	elemental analysis/wt% ^{a,b}						atomic ratio of P/V	valence of V ^d	composition
	V	P	C	H	N	O ^c			
HVPO	13.0 (13.0)	7.8 (7.0)	35.5 (34.9)	7.1 (8.2)	2.1 (2.1)	34.5 (34.8)	0.99	4.25	{C ₁₆ H ₃₃ N(CH ₃) ₃ } _{0.60} VP _{0.99} O _{4.90} ·3.45H ₂ O
CVPO	14.5 (14.4)	6.7 (6.7)	40.1 (40.1)	7.7 (8.4)	2.7 (2.5)	28.3 (27.9)	0.76	4.42	{C ₁₆ H ₃₃ N(CH ₃) ₃ } _{0.62} VP _{0.76} O _{4.42} ·1.74H ₂ O
LVPO	14.8 (14.7)	4.5 (4.5)	41.2 (40.7)	7.9 (9.1)	2.6 (2.5)	29.0 (28.5)	0.50	4.00	{C ₁₆ H ₃₃ N(CH ₃) ₃ } _{0.62} VP _{0.50} O _{3.56} ·2.64H ₂ O

^a No chloride was detected for each sample. ^b Numbers in parentheses were theoretical values calculated from composition. ^c 100 - sum of contents of V, P, C, H, and N. ^d Average valence of vanadium obtained by titration with KMnO₄.

**Figure 4.** TG curves and TPD mass spectra of mesostructured V-P-Os: (a) HVPO; (b) CVPO; (c) LVPO.

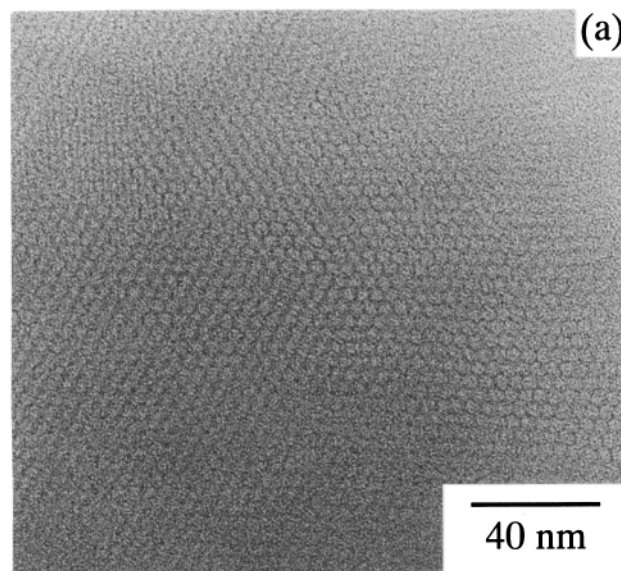
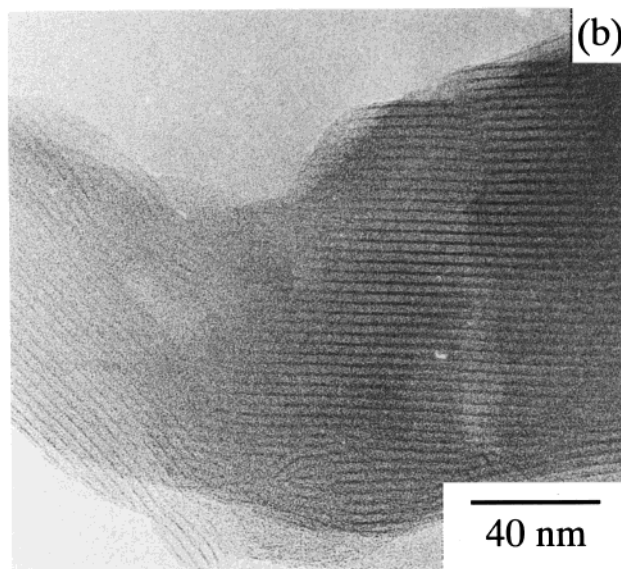
nm calculated with XRD data. The difference is probably due to the shrinkage of the structure by the electron beam irradiation.

The distance between two adjacent carbon atoms can be expressed by 0.127 nm/CH₂ in an all-trans extended alkyl chain,³⁴ and the length of C₁₆TMA is estimated to be 2.03 nm. The spacing of HVPO is 4.15 nm. The schematic packing of C₁₆TMA in the pore is proposed in Figure 6a.

There have been reported three kinds of hexagonally mesostructured V-P-Os with the P/V ratios of 0.5^{1,2} and 1.0.³ The former two have an amorphous wall, while the last one (ICMUV-2) has a crystalline wall. HVPO has the same P/V ratio as that in ICMUV-2, while the wall structures were different from each other.

II. Cubic-Mesostructured V-P-O. The amounts of V, P, C, H, N, and O were 14.5, 6.7, 40.1, 7.7, 2.7, and 28.3 wt %, respectively, as shown in Table 1. The P/V ratio was 0.76 and the average valence of V was 4.42. These values were different from those for HVPO. On the basis of these data, the chemical formula was estimated to be {C₁₆H₃₃(CH₃)₃}_{0.62}VP_{0.76}O_{4.42}·1.74H₂O.

The TGA and TPD mass spectra of CVPO are shown in Figure 4b. Below 503 K desorption of water was only observed and the corresponding weight loss was ≈9 wt

**Figure 5.** TEM photographs of hexagonal- and lamellar-mesostructured V-P-Os: (a) HVPO; (b) LVPO.

%, while the weak signals corresponding to the decomposition of C₁₆TMA were observed. The water content of 9 wt % was in agreement with 8.9 wt % in the chemical formula.

Figure 2b shows the XRD pattern of CVPO formed at pH 3.36. The observed reflection pattern was similar to that for silica MCM-48.^{5,11} Ten signals were observed at 2θ = 2.53°, 2.92°, 3.88°, 4.11°, 4.63°, 4.85°, 5.06°,

(34) Cao, G.; Mallouk, T. E. *Inorg. Chem.* **1991**, *30*, 1434.

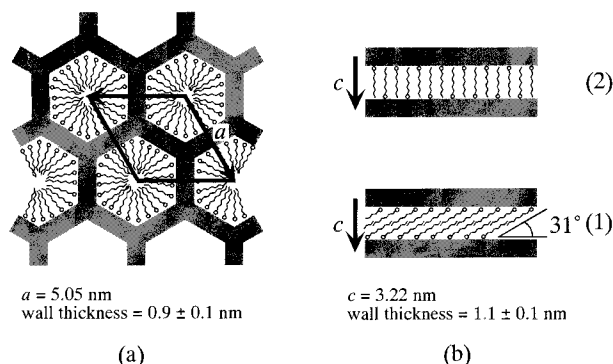


Figure 6. Schematic illustration of mesostructured V-P-Os: (a) HVPO; (b) LVPO. Regarding LVPO, there are two possible packing methods of C₁₆TMA.

5.24°, 6.50°, and 7.12°, assignable to (211), (220), (321), (400), (420), (332), (422), (431), (620), and (444) reflections of the cubic-mesostructured phase, respectively. The unit cell constant (*a*) was 8.54 nm. No signals other than those of CVPO were observed, suggesting the high purity of CVPO. This is the first report of the formation of cubic-mesostructured V-P-O. The signals were well resolved in comparison with the other mesostructured cubic materials of non-silica oxides, suggesting the higher crystallinity of CVPO.^{6,17,18,21}

In the range of 1300–500 cm⁻¹, the IR spectrum of CVPO exhibited an absorption band around 1015 cm⁻¹ with weak shoulder peaks at 1037, 1006, and 910 cm⁻¹, characteristic of V-P-O (Figure 3b). The bands were rather well resolved compared with those of HVPO, supporting the higher crystallinity. Unfortunately, attempts to observe a cubic pore system by TEM measurements were unsuccessful, probably because of the complicated pore system of the cubic mesostructure.^{35,36}

III. Lamellar-Mesostructured V-P-O. The results of elemental analyses for LVPO are summarized in Table 1. The amounts of V, P, C, H, N, and O in LVPO were 14.8, 4.5, 41.2, 7.9, 2.6, and 29.0 wt %, respectively, as shown in Table 1. The valence of V and P/V ratio were 4.00 and 0.50, respectively. On the basis of these data, the chemical formula was estimated to be {C₁₆H₃₃(CH₃)₃}_{0.62}VP_{0.50}O_{3.56}·2.64H₂O.

The TGA and TPD mass spectra of LVPO are shown in Figure 4c. Below 523 K desorption of water was only observed and the corresponding weight loss was 14 wt %, while the signals corresponding to the decomposition of C₁₆TMA were observed above 523 K. The water content of 14 wt % was in agreement with 13.7 wt % in the chemical formula.

The IR spectrum of LVPO is shown in Figure 3c. LVPO showed bands at 1111, 1098 (shoulder), 1072, 1014, 994, 966, 904, 722, 601, 543, and 503 cm⁻¹. The bands were sharper than those for HVPO and CVPO. The well-resolved IR bands suggest that the wall of LVPO is more crystalline than those of HVPO and CVPO.

The LVPO obtained at pH 3.45 gave intense diffraction signals at 2.74°, 5.53°, and 8.33° as shown in Figure 2c. These signals were assignable to (001), (002), and (003) reflections of the lamellar phase, respectively, and

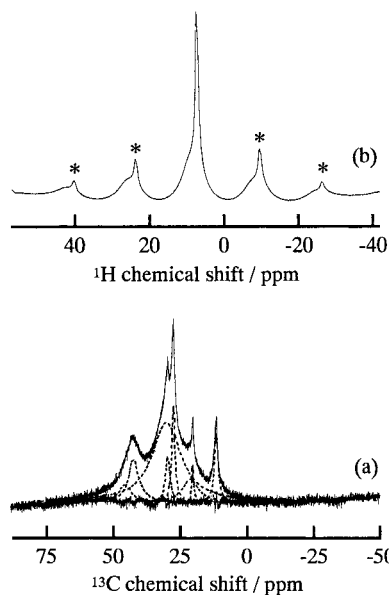


Figure 7. ¹³C and ¹H MAS NMR spectra of LVPO: (a) ¹³C MAS NMR spectrum. The spectrum is deconvoluted into eight lines shown by broken lines because the spectrum could not be well reproduced by using fewer bands. Sum of eight lines is shown by the solid line. (b) ¹H MAS NMR spectrum. Asterisks denote spinning sidebands.

the unit cell constant (*c*) was 3.22 nm. Weak signals were also observed at $2\theta = 11.04^\circ, 16.78^\circ, 19.49^\circ, 22.16^\circ, 24.52^\circ,$ and 27.38° , assignable to (004), (006), (007), (008), (009), and (0010) reflections, respectively. The rather high signal intensity at 19.49° may be due to the overlap with signals of wall structure.³⁷

The layered topology of LVPO was confirmed by TEM measurement as shown in Figure 5b. The thickness of layers and the interlamellar spacing were estimated to be 1.1 ± 0.1 and 2.1 ± 0.1 nm, respectively. The sum was 3.2 ± 0.1 nm, in fair agreement with the value calculated by XRD data.

The schematic packing of C₁₆TMA in the spacing of LVPO is proposed in Figure 6b, (1) and (2). Taking into account the interlamellar spacing of 2.12 nm and the length of C₁₆TMA of 2.03 nm, C₁₆TMA molecules can be packed in two ways: (1) double layer with a tilt angle of ≈31° (Figure 6b(1)) or (2) interdigitated monolayer (Figure 6b(2)).³⁴ The ¹³C NMR spectrum of C₁₆TMA bromide in CDCl₃ shows signals at 14.12, 22.68, 23.25, 26.24, 29.36–29.69, 31.92, 53.41, and 66.80 ppm corresponding to C16, C15, C3, C2, C4–C13, C14, CH₃(–N), and C1 (–CH₂(–N)), respectively.³⁸ The solid-state ¹³C MAS NMR spectrum of LVPO is shown in Figure 7a. The spectrum was deconvoluted into eight signals 12.29 (Δ*v*_{1/2}, 124 Hz), 20.92 (50), 21.73 (512), 28.19 (102), 30.45 (150), 30.90 (986), 43.38 (349), and 46.63 (424) ppm, assignable to C16, C15, C3, C2, C14, C4–C13, CH₃(–N), and C1, respectively. The signal positions of CH₃–N and C1 carbons were shifted more to a higher field while the C16 signal position did not change much. The signals in Figure 7a were broader than those of C₁₂–

(35) Alfredsson, V.; Anderson, M. W. *Chem. Mater.* **1996**, *8*, 1141.

(36) Alfredsson, V.; Anderson, M. W.; Ohsuna, T.; Terasaki, O.; Jacob, M.; Bojrup, M. *Chem. Mater.* **1997**, *9*, 2066.

(37) Attempts to determine the wall structure have been unsuccessful by using the Cerius2 program with previously known structures of V-P-Os such as [N(CH₃)₄]V₃O₇, VOPO₄, VOHPO₄·0.5H₂O, and (VO)₂P₂O₇.

(38) Spectral data was available from <http://www.aist.go.jp/RIODB/SDBS/> (June 17, 2000).

TMA and C₁₆TMA in MCM-41^{4,39,40} or in their solid states, and among them the CH₃(-N) and C1 signals were much broader. Broad signals were also observed for ¹H MAS NMR as shown in Figure 7b. The broadness probably comes from paramagnetic V⁴⁺ in LVPO. The large shift and broadness of ¹³C signals of CH₃(-N) and C1 suggest that these alkyl groups are close to V⁴⁺. On the other hand, the extent of broadening of the C16 methyl signal was much smaller than those of the other carbons and the position did not change much, suggesting weak interaction of the carbon with V⁴⁺ and that these sites are far from each other. Therefore, Figure 6b(1) is more probable.

Haskouri et al. have reported lamellar-mesostructured V-P-O with the crystalline wall of VOPO₄.⁴¹ The P/V ratio was 1.0 and different from the 0.5 of LVPO, indicating that these two materials were different from each other. The difference in IR spectra supports the idea.

Removal of C₁₆TMA. The mesostructures of HVPO, CVPO, and LVPO were collapsed by removing C₁₆TMA templates with the calcination in N₂ or air. However, the removal of the C₁₆TMA by ion exchange was possible for LVPO as follows. After C₁₆TMA in LVPO was exchanged with K⁺, the IR spectra of resulting materials showed bands at 1116, 1063, 1046, 1009 (shoulder), 1001, 976, 960, 938, 911, 700, 614, 545, and 513 cm⁻¹ as shown in Figure 8a. The IR spectrum showed a pattern similar to that of LVPO in Figure 3c except for the disappearance of the bands around 1470 cm⁻¹ of C₁₆TMA. The original XRD signals for LVPO disappeared and new signals were observed for the K⁺-exchanged sample at 2θ = 8.5°, 16.5°, and 25.9° corresponding to *d* spacings of 1.03, 0.54, and 0.37 nm, respectively, as shown in Figure 8b. It was confirmed by XRD that the ion exchange of C₁₆TMA with K⁺ was completed after 2 h. The unit cell constant calculated with XRD data was 1.0 nm. Similarly, the C₁₆TMA could be exchanged with Cs⁺ and the resulting Cs⁺-exchanged sample showed XRD signals at 2θ = 7.79°, 15.75°, and 22.31° corresponding to *d* spacings of 1.13, 0.56, and 0.40 nm, respectively. These facts show that C₁₆TMA templates are exchanged with K⁺ or Cs⁺.

The exchange of C₁₆TMA with K⁺ was also supported by the following facts. The amounts of V, P, and K in K⁺-exchanged LVPO were 33.0 ± 1.3, 11.9 ± 0.4, and 8.7 ± 0.5 wt %, respectively. The atomic ratios of P/V and K/V were 0.59 ± 0.04 and 0.35 ± 0.03, respectively. The P/V ratio approximately agreed with that of the original LVPO while the K/V ratio was a little smaller

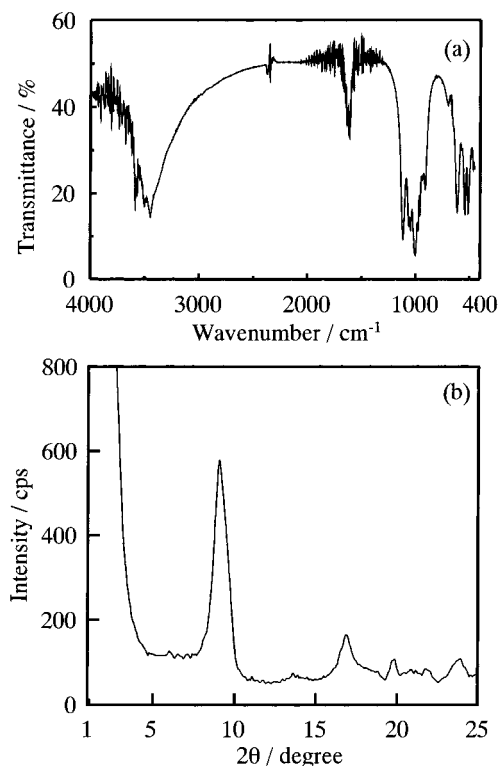


Figure 8. IR spectrum and XRD pattern of LVPO after the exchange of C₁₆TMA with K⁺: (a) IR spectrum; (b) XRD pattern.

than the ratio of C₁₆TMA/V in the original LVPO. The color of LVPO was bluish green and changed to dark green during the K⁺ exchange. The color change to dark green is probably due to the mixing of V⁴⁺ and V⁵⁺.⁴² Therefore, the difference between K/V and C₁₆TMA/V ratios is probably due to the partial oxidation of V⁴⁺ into V⁵⁺ during the exchange reaction in air. Such a similar difference was also observed for the Cs⁺ exchange. The exchange with Li⁺ was unsuccessful.

The BET surface area of K⁺-exchanged LVPO was 10 m² g⁻¹. By evacuation at 573 K the surface area was 12 m² g⁻¹ and was not changed much. The XRD signal at 2θ = 8.5° was observed. The XRD signal at 2θ = 8.5° disappeared and the IR spectrum significantly changed by evacuation at 673 K. These results show that K⁺-exchanged LVPO was stable at 573 K, but the structure decomposed at 573 K.

Acknowledgment. We acknowledge Prof. Emeritus M. Misono (Kogakuin University) for his encouragements of this work. This work was partly supported by a Grant-in-Aid for Scientific Research from the Ministry of Education, Science, Sports and Culture of Japan.

CM000524Y

(39) Kolodziejski, W.; Corma, A.; Navarro, M.-T.; Pérez-Pariente, J. *Solid State Nucl. Magn. Reson.* **1993**, *2*, 253.

(40) Beck, J. S.; Vartuli, J. C.; Kennedy, G. J.; Kresge, C. T.; Roth, W. J.; Schramm, S. E. *Chem. Mater.* **1994**, *6*, 1816.

(41) Haskouri, J. E.; Cabrera, S.; Roca, M.; Alamo, J.; Beltrán-Porter, A.; Beltrán-Porter, D.; Marcos, M. D.; Amorós, P. *Inorg. Chem.* **1999**, *38*, 4243.

(42) Schindler, M.; Hawthorne, F. C.; Baur, W. H. *Chem. Mater.* **2000**, *12*, 1248.